JOURNAL OF GEOPHYSICAL RESEARCH, VOL. 112, B09302, doi:10.1029/2006JB004542, 2007

Application of the telegraph model to coda Q variations in southern California

Paul M. Davis[1] and Robert W. Clayton[2]

Received 26 May 2006; revised 27 November 2006; accepted 3 May 2007; published 11 September 2007.

[1] We examine waveforms and data used to construct coda magnitude in southern California to estimate the spatial variation of coda Q and its dependence on frequency. Our analysis combined with independent borehole data suggests that coda is mainly generated by multiple scattering in the upper few kilometers of the crust where large impedance contrasts occur because of surface layering or fracturing. The ubiquitous observation that coda Q increases with frequency is explained as arising from multiple reverberations in the upper crust. We suggest that the telegraph model that has been successfully used to describe reflection seismogram multiples in the exploration industry may also apply to earthquakes. Under this model the apparent increase of Q with frequency is due to trapping of high-frequency energy in the upper crust. This behavior is expected if the associated reflector series has an exponential autocorrelation function, a feature of the telegraph model. At lower frequencies, trapping is less efficient. The combined effects give rise to an apparent absorption band that we suppose is superimposed on frequency-independent intrinsic attenuation. Maximum apparent attenuation occurs at wavelengths equal to the dimensions of the regions of upper crust that contain the scattering layers. At lower frequencies, trapping is less effective, and attenuation decreases as the longer-wavelength waves sample the deeper crust and upper mantle where because of overburden pressures, acoustic impedance contrasts are less extreme. By taking spectral ratios of coda waves to direct S, we estimate that intrinsic Q is high ($\sim$3000) and that coda may be modeled as multiple scattered S waves in a region of anisotropic scattering. The exponential decay of the coda is a result of the perfectly reflecting surface of the Earth with backscattering from random near-surface layers causing progressive leakage and loss of energy downward into the more transparent lower crust and mantle.

Citation: Davis, P. M., and R. W. Clayton (2007), Application of the telegraph model to coda Q variations in southern California, *J. Geophys. Res.*, *112*, B09302, doi:10.1029/2006JB004542.

1. Introduction

[2] Coda decay has been used as a measure of the magnitude of seismic sources including earthquakes and explosions. The coda is thought to be due to scattering of direct waves from heterogeneities in the crust and mantle [*Aki*, 1980]. Being an integrated measure of scattering effects, it has proved to be a robust estimator of source strength, as it averages out focal mechanism and local focusing-defocusing effects, both of which affect body wave amplitudes. However, the nature of the coda decay has been controversial. Models have been proposed that describe it as a combination of scattering and absorption, and the models differ as to the distribution of scatterers and whether absorption or scattering, or both, dominate the decay [*Aki and Chouet*, 1975; *Frankel and Wennerberg*, 1987]. The standard approach is to distribute the scatterers randomly in an infinite isotropic medium, to integrate the scattered wavefield under various approximations, such as weak scattering from small impedance contrasts, and to sum the effects of single or multiple scattering. Understanding the physics of coda decay is important if reliable estimates of earthquake size or explosion yield are to be made.

[3] Since the late 1970s, coda envelopes measured at stations of the Southern California Seismic Network for a given event have been fit to a simple power law decay comprised of two parameters: an amplitude term and the power law exponent. These parameters have been stored in the Southern California Earthquake Data Center (SCEDC) and can be used to reconstruct smoothed coda envelopes. By restricting the analysis to narrow magnitude bands, the coda decay, and hence coda Q, can be estimated as a function of frequency. Digital waveforms have been stored for a subset of these data, with the most complete set after the year 2000. We make estimates of coda Q using both data sets, which serves as a comparison, as well as adding data for stations for which waveforms are not available.

[1]Department of Earth and Space Sciences, University of California, Los Angeles, California, USA.
[2]Seismological Laboratory, California Institute of Technology, Pasadena, California, USA.

0148-0227/07/2006JB004542$09.00

[4] We use the coda Q values to test the hypothesis that scattering concentrates in the uppermost crust where impedance contrasts are greatest either due to sedimentary or metamorphic layering and where, by virtue of lower overburden pressure, damage caused by past tectonic events has generated significant heterogeneity. We describe the scattering by the telegraph model, a model that was originally developed for telecommunications [e.g., *Papoulis*, 1965]. Originally, telegraph signals relied on switching the carrier, or voltage, on and off to transmit signals, such as Morse code. A random telegraph wave has two states and switches between them at random moments. The telegraph model has been effective in describing, in a statistical sense, the effects of stratigraphic sequences on reflection seismograms used in exploration geophysics [*Banik et al.*, 1985b].

2. Coda Models

[5] The earliest models of scattering [e.g., *Pekeris*, 1947; *Chernov*, 1960; *Wu and Aki*, 1988] calculated the wavefield generated by single scattering from randomly distributed heterogeneities in an infinite elastic medium assuming that impedance contrasts are small enough that the Born approximation can be applied. Noting that the Born approximation does not conserve energy, *Frankel and Wennerberg* [1987] and *Zeng et al.* [1991] generalized scattering models to include multiples in formulations constrained to overcome this limitation. *Frankel and Wennerberg*'s [1987] model describes coda decay as mainly due to intrinsic absorption. *Zeng et al.*'s [1991] model has been used to describe absorption and scattering effects in coda [*Hoshiba*, 1991; *Mayeda et al.*, 1992; *Koyanagi et al.*, 1992; *Jin et al.*, 1994] by matching coda decay at multiple stations and multiple time steps. That approach purports to analyze sufficient data to separate absorption effects, described by intrinsic Q_I, and scattering effects, described by scattering Q_S, as a function of frequency. In general, it is found that both Q increase with frequency and $Q_I \approx Q_S$. This observation is in sharp contrast with experiments on most materials for which intrinsic Q is frequency-independent [e.g., *Knopoff*, 1964].

[6] *Aki* [1980] used the weak scattering model to describe coda Q_C as a combination of intrinsic and scattering Q given by

$$\frac{1}{Q_C} = \frac{1}{Q_I} + \frac{1}{Q_S}. \tag{1}$$

When geometric spreading is taken into account [*Aki and Chouet*, 1975], the coda envelope is given by

$$y(t) = \frac{A}{t}\exp(-\omega t/2Q_C), \tag{2}$$

where A is a constant, t is time, and ω is angular frequency. This model, based on single-scattering and the Born approximation, is sometimes referred to as Chernov scattering [after *Chernov*, 1960]. To improve on the Born approximation, *Frankel and Wennerberg* [1987] described a multiple-scattering model that conserves total energy. They found that

$$y(t) = Bt^{-3/2}\left(1 - e^{-\omega t/2Q_S}\right)^{1/2} \tag{3}$$

gives a satisfactory fit to synthetic seismograms calculated by finite differences (based on a method by *Frankel and Clayton* [1986]), where B is a constant. Their model makes the assumption that because of multiple scattering, the scattered field is uniformly distributed across the volume contained within the expanding spherical wavefront, so that the scattering energy per unit volume decreases as t^{-3}. Simultaneously, scattering causes the energy in the direct wave to decrease as $\exp(-\omega t/Q_S)$ which transfers into the scattered field as $1 - \exp(-\omega t/Q_S)$. Combining these effects, the scattered energy evolves as $1/t^3\ (1 - \exp(-\omega t/Q_S))$. Converting to amplitude by taking the square root with an additional term to account for absorption, they obtained

$$y(t) = Bt^{-3/2}\exp(-\omega t/2Q_I)[1 - \exp(-\omega t/Q_S)]^{1/2} \tag{4}$$

for the temporal variation of the coda envelope. Because of the square root the coda decay is mostly dependent on Q_I. If Q_S is large, equation (4) has the same temporal behavior as equation (2) because to first order the term with the square root becomes proportional to $t^{1/2}$.

[7] The variation of Q_S with frequency depends on the statistics of the scatterers. A power spectrum [e.g., *Dainty*, 1981; *Wu and Aki*, 1988] gives rise to power law behavior of $Q(\omega)$, with no intrinsic scale, whereas a Gaussian spectrum [*Padhy*, 2005] or reflector series with an exponential autocorrelation function [*Banik et al.*, 1985a] gives rise to absorption bands that peak at the scale length determined by the distribution.

3. Converting Coda Magnitude Data to Coda Decay

[8] In order to compare predictions of the various theories and to examine the spatial variation of coda Q as a function of frequency, an analysis of multiple seismograms at multiple stations is required. We began this research by reconstructing smoothed versions of coda envelopes that have been stored in highly compressed form as a by-product of routine coda magnitude calculations in southern California. These envelopes were then used to estimate coda Q and are compared with estimates from waveforms in section 4. We assumed that coda Q determined for different earthquake sizes would give values representative of different frequencies determined by corner frequency. To eliminate local site effects, as well as station frequency response, our estimates were made by analyzing the coda at a given station for all earthquakes in a narrow magnitude range within 40 km of the station. The decay of the coda envelopes with distance for a restricted magnitude range is used to obtain Q.

[9] Coda magnitude, m_C, is measured at 232 stations of the Southern California Seismic Network (Figure 1) by fitting the coda decay after the S wave by an empirical function

$$y = \frac{10^{m_C + a_0}}{\tau^q}, \tag{5}$$

where $\tau = t - t_P$, t is time, t_P is time of arrival of the P wave, m_C is coda magnitude, and q and a_0 are parameters that are adjusted at each station to obtain a common m_C. Equation (5) is fit to averages of the (on-scale) coda envelope taken

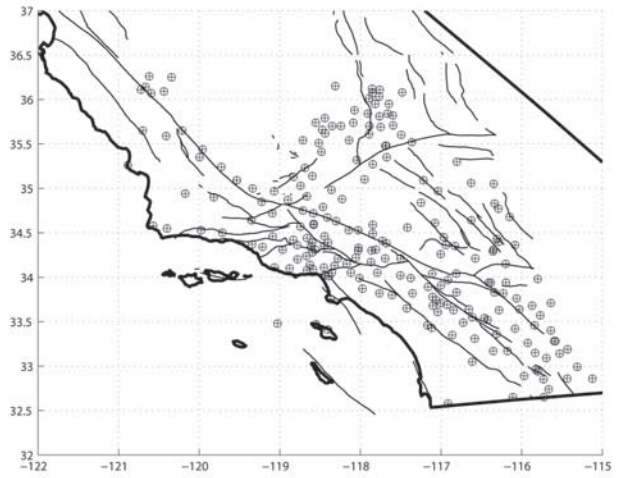

Figure 1. Map of southern California seismic network stations used in coda Q analysis.

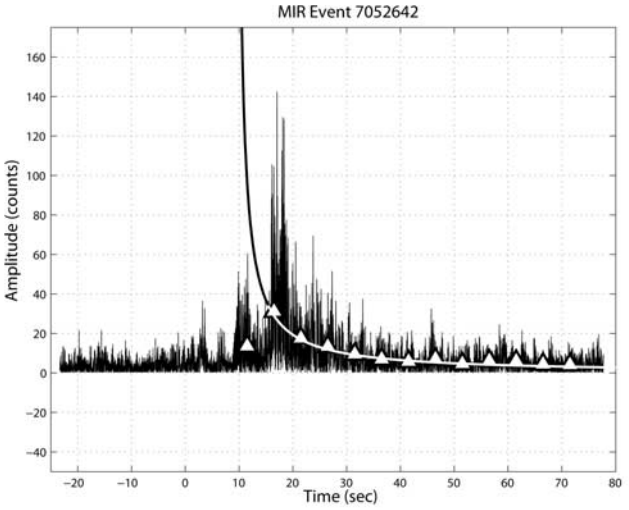

Figure 2. Fit of equation (5) to 5-s averages of coda (y axis digitizer counts) after the S wave for a magnitude 2.2 earthquake using the tabulated a and q values (for station MIR, Martinez Indian Reservation). The triangles are 5-s averages of the absolute value of the waveform. The second triangle from left marks the arrival of the S wave. The solid line is calculated from equation (5) using tabulated a and q values. The excellent fit to the data verifies our interpretation of these values.

over ~5-s intervals starting at the S wave arrival t_S [*Johnson*, 1979]. An example for a magnitude 2 earthquake is shown in Figure 2.

[10] We reconstructed coda envelopes for multiple (several million) events over narrow magnitude ranges by dividing up the $[a_i, q_i]$ for a given station into seven magnitude bins m_C = [2.0–2.2, 2.2–2.4, 2.4–2.6, 2.6–2.8, 2.8–3.0, 3.0–3.2, and 3.2–3.6]. The higher magnitude ranges ($m_C > 3.6$) cause the short-period stations to saturate and so did not provide enough data for curve fitting.

[11] Since the seismometers are velocity transducers, spectra from individual earthquakes are peaked at the event's corner frequency [*Brune*, 1970] provided that the bandwidth is wide enough. Two seismic channels are used for coda Q estimates, the extremely short-period high-gain vertical (EHZ) and high-broadband high-gain (HHZ) channels. The frequency response of the EHZ channel is flat to velocity to about 25 Hz. To estimate representative frequencies for the different magnitude bands, we compared peak frequency as a function of magnitude by fitting a Gaussian to the fast Fourier transform (FFT) amplitudes of waveforms from the EHZ and HHZ channels for a representative set of stations (Figure 3). For the EHZ channel the combination of short-period bandwidth and corner frequency resulted in spectral at frequencies that peaked at [10.5, 8.0, 6.0, 4.6, 3.4, 2.2, 1.2] Hz, corresponding to the above magnitude ranges, respectively, whereas for the HHZ channels this range is [18, 16, 14, 12, 10, 8, 6] Hz.

[12] The values for the HHZ channels are similar to the corner frequencies, whereas those for the EHZ channels are about half the respective corner frequencies. This discrepancy occurs because the combination of "extremely short period," channels with a low-pass frequency of 25 Hz from the analog data transmission, results in a short-period filter.

[13] We then calculated the coda envelope value at twice the lapse time (twice the S wave traveltime) for all the events for a given station. We used events that were less than 40 km distant from the station in order to restrict the analysis to body waves and to avoid surface waves which

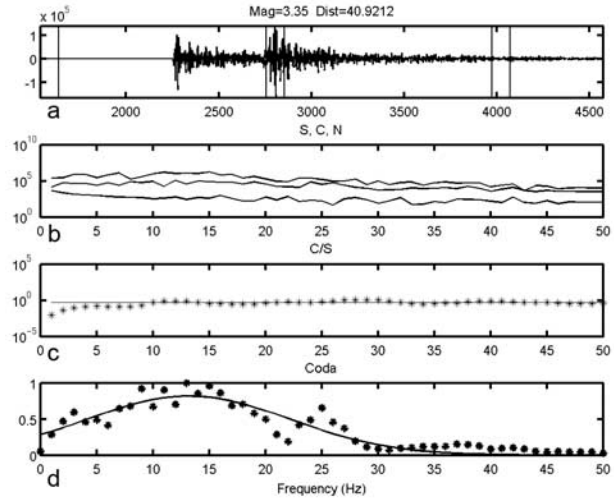

Figure 3. Measuring representative frequencies as a function of magnitude bands. (a) Seismogram (HHZ channel station RDM) with 1-sec windows N, S, and C marked by the vertical lines left to right, where N is noise, S is S wave and C is coda at twice the lapse time. (b) Spectral amplitudes of selected windows of the seismogram shown in Figure 3a. Top curve is the log amplitude spectrum of the S wave. Lower curve is that of the coda and lowest curve is the noise. (c) Spectral ratio (stars) of the Coda to S waves showing that the ratio is effectively flat, consistent with high intrinsic Q. The solid curve is the average ratio. (d) Gaussian fit to the coda spectral amplitudes (stars) as a function of frequency (linear plot).

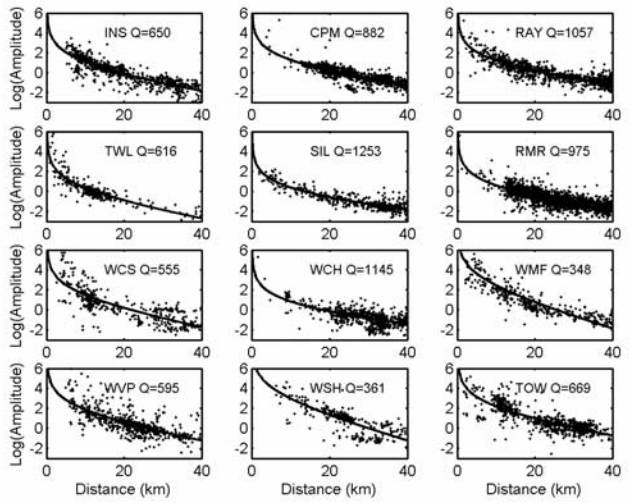

Figure 4. Coda amplitudes at various stations of the Southern California Seismic Network estimated from equation (6) at twice the lapse time plotted as a function of distance (km). The solid lines are least squares fits of equation (7) for the magnitude range 2.0–2.2 (f = 10.5 Hz). Values of coda Q estimated from the exponential decay are about 800–1000.

would have a $1/t^{1/2}$ geometric spreading rather than $1/t$. Twice the lapse time is used so that scattering effects are well developed. Substituting in equation (5) for a given station, we obtain the amplitude, y_i, of the coda for the ith earthquake as

$$y_i = \frac{10^{M_{C_i}+a_{0_i}}}{(2t_{S_i} - t_{P_i})^{q_i}}. \tag{6}$$

These data can be used as input to a least squares inversion to solve for the Q values in either (2) or (4). For example, using equation (2),

$$y_i = \frac{10^{M_{C_i}+a_{0_i}}}{(2t_{S_i} - t_{P_i})^{q_i}} = \frac{A}{2t_{S_i}} \exp(-\omega 2t_{S_i}/2Q_C). \tag{7}$$

Taking the logarithm of (7),

$$\ln(y_i) - \ln(2t_{S_i}) = \log(A) - \omega 2t_{S_i}/2Q_C. \tag{8}$$

Equation (8) is the equation of a straight line, which is fit to the data to determine $1/Q_C$. Alternatively, we use an iterative nonlinear inversion to fit Q_I and Q_S values from equation (4). Traveltimes of P and S waves were obtained from the Southern California Earthquake Center velocity model [*Magistrale et al.*, 2000] for the event-station paths. Equation (7) is plotted versus the y_i for a subset of the stations in Figure 4. The fits are quite noisy, but because of the order of 500 points are used, the parameters are reasonably well resolved. Many stations exhibited this level of fit. Stations were not used if the standard deviations of the fit were greater than 20% of the Q value. This occurred if either the number of earthquakes was too small or the earthquakes were too clustered to give a wide range of lapse times.

4. Coda Q Waveforms

[14] To check the coda magnitude method and to add independent measurements, we used waveforms in the M = 2–4 range for all available EHZ (extreme short-period high-gain vertical, 100 samples per second) channels, 1985 to present and all HHZ channels (high-bandwidth high-gain verticals) 2000 to present. We limited the maximum number of waveforms to 1000 events for each station. A program was written to identify all events in a 40 km radius of a station. Then these data were requested from the triggered channels of the SCEDC using the seismogram transfer program STP. A total of 188,052 seismograms were retrieved and analyzed for the 458 stations of the network, i.e., on average, 410 per station. Some reasons why this number is less than the requested 1000 include that some stations did not trigger, data were noisy, and a station was down for that time interval. Each seismogram was divided into 1-s windows to obtain samples of the noise, N, prior to the P arrival, S wave data, S, centered on the S wave arrival, and coda, C, at twice the S wave lapse time (Figure 3). The windowed data were demeaned, Fourier transformed, and converted to amplitude. For the coda analysis the $C(\omega)$ were corrected for noise energy using

$$C(\omega) \rightarrow \sqrt{C^2(\omega) - N^2(\omega)}. \tag{9}$$

The $C(\omega)$ were then averaged over frequency bands [1–3, 3–6, 6–9, 9–12, 12–15, 15–18, 18–21] Hz, and normalized by moment, M_0, using the moment magnitude relation $m = 2/3\log_{10} M_0 - 6.07$. We refer to these as the [2, 4.5, 7.5, 10.5, 13.5, 16.5, and 19.5] frequency bands. The resulting $C(\omega)$ were fit to

$$C(\omega) = \frac{a_1}{t} \exp\left(-\frac{\omega t}{2Q_C(\omega)}\right) \tag{10}$$

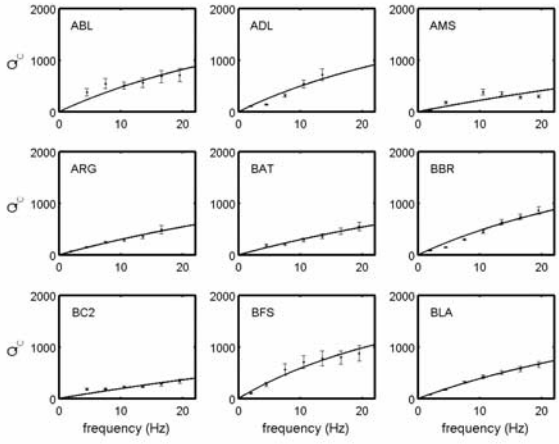

Figure 5. Coda Q as a function of frequency from coda waveforms. The approximately linear increase with frequency is consistent with the asymptotic behavior of the telegraph model and frequency-independent intrinsic Q.

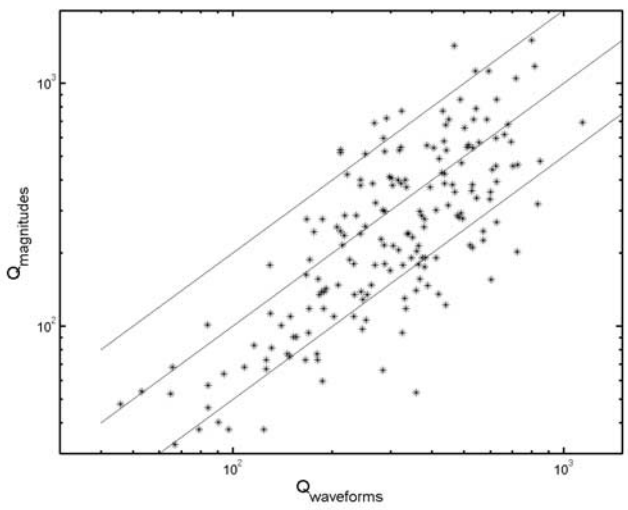

Figure 6. Log-log plot of coda Q determined from coda magnitudes versus coda Q from waveforms for estimates with $Q/\sigma > 5$. Solid lines correspond to $Q_{\text{magnitude}} = 2Q_{\text{waveforms}}$, $Q_{\text{magnitude}} = Q_{\text{waveforms}}$, and $Q_{\text{magntiude}} = 1/2Q_{\text{waveforms}}$, from top to bottom.

using equation (8) to find $Q_C(\omega)$ for all data for a given station in each frequency band. Stations were not used if the number of events in the spatial-temporal box was too small or if the ratio of Q to its standard deviation, σ, i.e., Q/σ was too low. The number of the 458 stations satisfying $Q/\sigma > 5$ for four or more frequency estimates was 169 stations, i.e., with errors less than 20%. The coda Q plotted as a function of frequency in Figure 5 show a linear dependence on frequency with a slight downward curvature that is discussed in section 6.

5. Comparison Between Coda Magnitude and Waveform-Derived Coda Q

[15] Comparison of the statistics of all fits of the coda magnitude and waveform methods (equation (8) or (10)) to amplitude decay gives a median standard deviation for the coda Q in each band about 40% and 26%, respectively, of the estimated values. The agreement between the two populations was not expected to be exact. A comparison between coda Q for each method is shown in Figure 6, where the data have been limited to $Q/\sigma > 5$. For some of the best determined stations the agreement was excellent, with 82% of the values within 50% of each other, but a range less than the 95% expected by these statistics. Both methods find that coda Q increases with frequency to first order in a linear fashion. Both also agree on the general trends that basins and the Salton Sea area have low Q, with mountainous areas having significantly higher Q. Figure 7 shows stations in the southern California network for which the magnitude and waveform methods had four or more frequency bands with $Q/\sigma > 5$. In general, the agreement between the two methods is good. LRM (Laurel Mountain) is an exception for which we do not have an explanation. We excluded the Coso network because many events saturated those sensors.

[16] This analysis was begun to test if the coda magnitude data could serve as a reliable and accessible method for obtaining coda Q as a function of frequency. Comparison

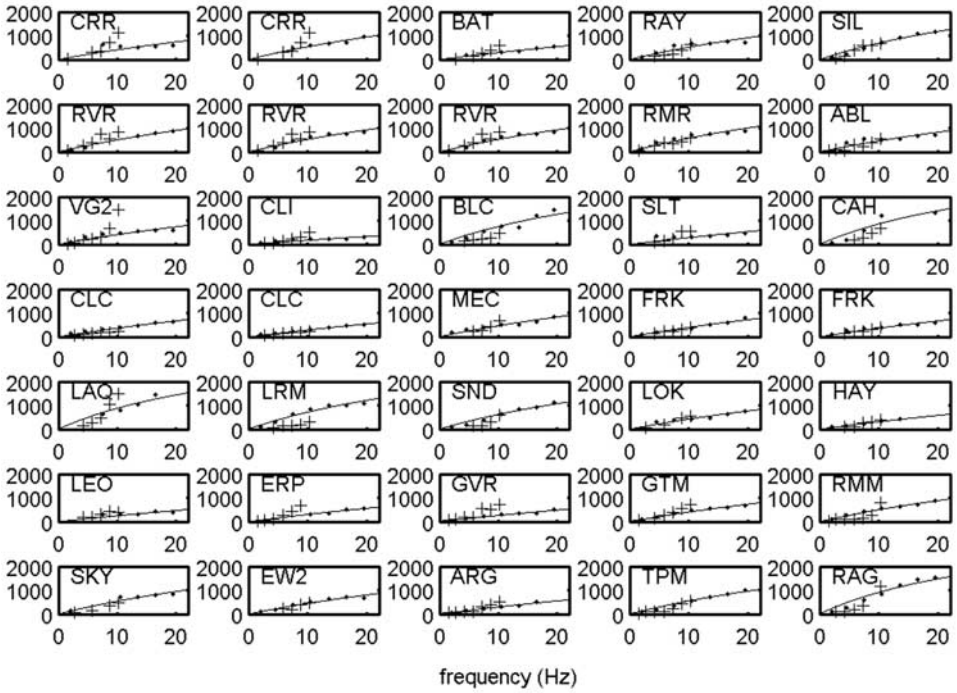

Figure 7. Comparison between $Q_{\text{magnitude}}$ (dots) and $Q_{\text{waveforms}}$ (pluses) for selected stations for which the determinations in both cases have a standard deviation of less than 20% of the Q values ($Q/\sigma > 5$). The solid curves are the combination of scattering Q and intrinsic Q from equation (12). Repeated stations are for estimates from either different channels (EHZ, HHZ) or time intervals.

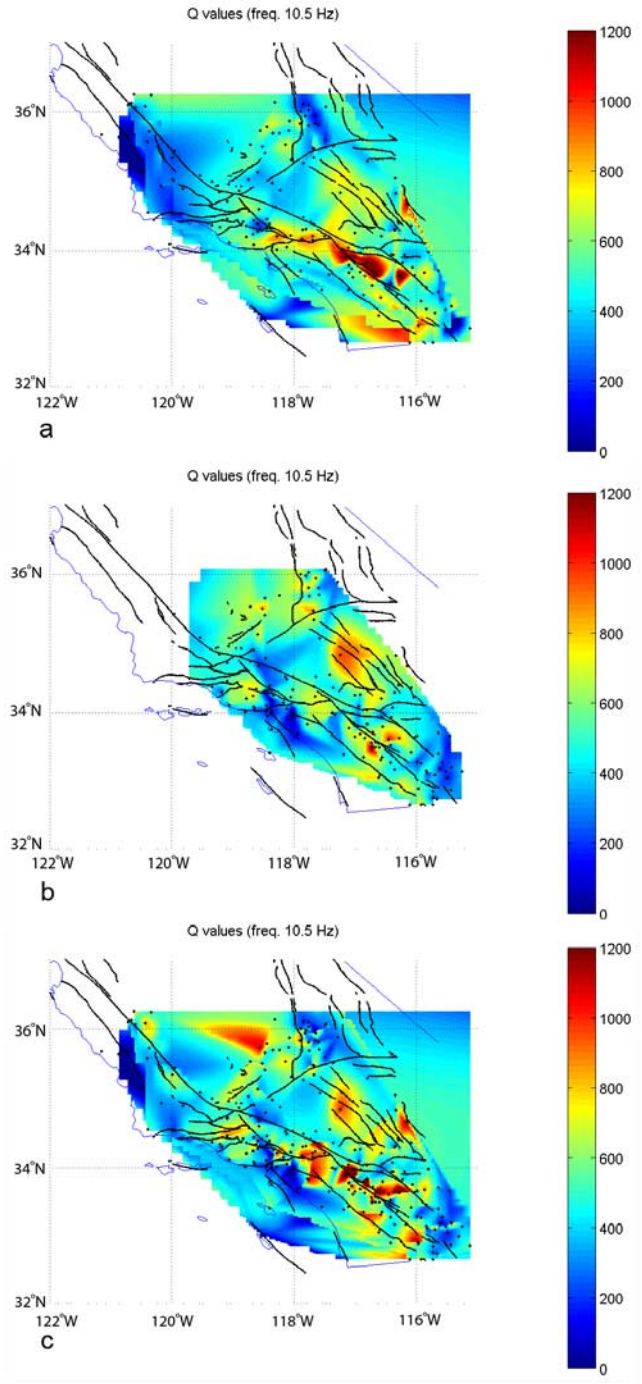

Figure 8. Maps of coda Q. (a) Magnitude-determined values for the magnitude range m_C = [2.0–2.2] corresponding to 10.5 Hz. (b) Waveform-determined values for the 9–12 Hz band. (c) Combined magnitude and waveform-determined values.

with direct waveforms reveals that although the coda magnitude method works satisfactorily, it gave more noisy results. It is not a substitute for using the waveforms themselves but can be used to obtain approximate estimates where waveform data have not been archived.

[17] As a final step in the analysis, smoothed spatial maps of the coda Q were constructed for comparison with the geology of the region. The coda Q output of the waveform and magnitude analysis is visualized in maps of coda Q shown in Figures 8a and 8b for the 10.5-Hz frequency band. The data used were restricted to those for which the standard deviation of the fit was less than 20% of the coda Q value. This restriction resulted in 122 magnitude-based stations and 169 waveform-based stations. The maps show a similar range of values and spatial variation, bearing in mind that individual estimates are accurate to 20%. The combined plot is shown Figure 8c. The maps use the Matlab program Griddata with cubic interpolation. Thus the color is only accurate at the station locations themselves, but it serves to highlight clusters of stations with similar values.

6. Discussion

[18] Both methods of analysis show that coda Q increases nearly linearly with frequency with a slight downward curvature seen in the high-frequency data from the waveform analysis. These results are consistent with observations elsewhere. A compilation of coda Q results from around the world [*Padhy*, 2005] shows that the data are well fit by an absorption band ($1/Q$) peaked at about 0.5 Hz. The associated Q variation, the inverse of the absorption, has high values at DC decreasing to a minimum at 0.5Hz, after which it initially increases linearly and then curves to become asymptotic to a constant value at high frequency. All of Padhy's reported measurements are on the high-frequency side of the absorption peak, as are ours ($f > 2$ Hz), while the low-frequency Q are inferred from long-period body and surface waves but are not well resolved.

[19] A number of scattering models have been proposed that can explain the observed variation with frequency [e.g., *Dainty*, 1981; *Wu and Aki*, 1988]. If the heterogeneities in the crust have a power spectrum given by $P(k) = k^{-m}$, where k is wave number, then weak scattering models find [*Wu and Aki*, 1988]

$$\frac{1}{Q} = \frac{1}{Q_0}\omega^{1-m}, \tag{11}$$

$m = 1$ corresponds to frequency-independent Q while $m = 2$ has Q, increasing linearly with frequency. In either case, an absorption band is not predicted. A candidate model that appears in the literature, which exhibits absorption band behavior, is the telegraph model. The telegraph model as applied to reflection seismology describes multiple scattering within layering that has a reflector series with an exponential autocorrelation function [e.g., *Banik et al.*, 1985b]. The attenuation of the telegraph model is given by a function of the form

$$\frac{1}{Q(\omega)} = \frac{2}{Q_{\min}} \frac{\omega/\omega_c}{1 + (\omega/\omega_c)^2}, \tag{12}$$

where ω_c is given by 2/(average travel-time) in the layers [*Banik et al.*, 1985b] and $Q_{\min}$, which corresponds to maximum apparent absorption (minimum Q) from destructive interference of the scattered signals, occurs at $\omega = \omega_c$. It has been noted that equation (12) has identical frequency dependence to that of the standard (viscoelastic) solid and as

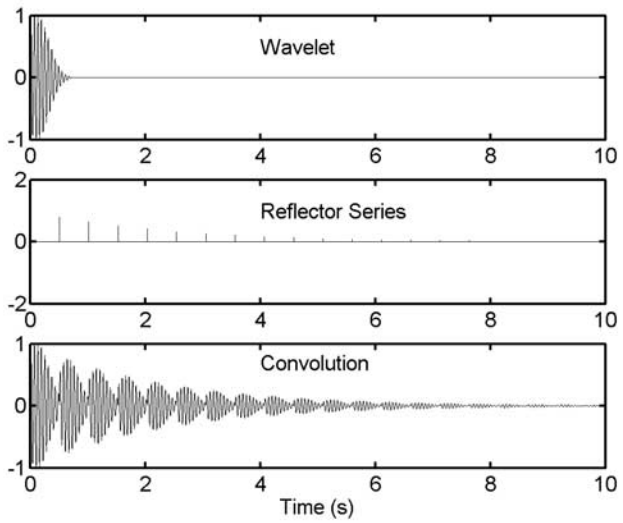

Figure 9a. A high-frequency wavelet (top) convolved with the reflector series to generate a simple synthetic seismogram which, because of multiple reflections, has high apparent Q.

Wennerberg and Frankel [1989] note, it is not possible to resolve between them on the basis of frequency dependence of Q. In making a choice we appeal to attenuation results from deep borehole seismometers.

[20] Our choice of the telegraph model was predicated on the observations that Q effects in boreholes are greatest near the surface. In the early 1990s, seismograms were measured at various depths in a 3-km-deep borehole in Cajon Pass, California [*Abercrombie*, 1995, 1997, 1998], which revealed that attenuation concentrates toward the surface. Similar results were found in boreholes up to 1 km deep in Parkfield, California [*Abercrombie*, 2000]. *Abercrombie* [1998, p. 481] finds that for an "earthquake recorded at Cajon Pass wellhead, with a hypocentral distance reaching 15 km, over 90% of the attenuation would occur in the upper 3 km, 80% in the upper 1.5 km, and 50% in the upper 300 m (at frequencies of a few Hz and above)." At 2.5 km depth, *Abercrombie* [1998, p. 481] finds that spectra from distant local earthquakes exhibit the "exponential fall-off predicted by the frequency-independent Q model used over two decades of frequency bandwidth," whereas Q from surface data exhibited a strong frequency dependence below 10 Hz ($\omega^{1.8}$) but at higher frequencies, the frequency dependence weakens ($\omega^{0.34}$) [*Adams and Abercrombie*, 1998]. It is generally recognized, using shallow borehole data, that a considerable fraction of the attenuation between an earthquake and the surface occurs in the upper hundreds of meters [*Assimaki et al.*, 2006]. We conclude that the borehole surface data exhibit the absorption band behavior that we see in our coda magnitude analysis. The fact that the frequency dependence of Q is absent, or less obvious, at depths greater than 3 km suggests that the coda Q obtains its frequency dependence in the upper 3 km, probably concentrated toward the surface. We further argue that since multiple scattering is necessary for generation of the coda durations that last many tens of seconds from earthquakes with a source time of a fraction of a second, it can also explain the inferred absorption band.

[21] The telegraph model has been shown to adequately describe the statistics of impedance variation with depth that consists of a sequence of uncorrelated random steps. The impedance remains constant between steps for intervals with lengths determined by the (Poisson) probability of no change in an interval, t, proportional to $e^{-\omega_c t/2}$. The attenuation is given by equation (12). The telegraph model is a smoothed version of the *O'Doherty and Anstey* [1971] result that for multiple reflections the log amplitude spectrum of the transmitted pulse, T, equals the power spectrum of the reflection coefficient series R,

$$T(\omega) = \exp[-R(\omega)t], \tag{13}$$

which gives Q as

$$\frac{1}{Q} = \frac{2R(\omega)}{\omega}. \tag{14}$$

[22] The telegraph model has used successfully to relate seismograms measured at the surface to the reflection series obtained from borehole logging. A formal proof of equation (13) was provided by *Banik et al.* [1985a] that supplemented the heuristic derivation of the original authors. *Banik et al.* [1985b] tested equation (13) against well log data from the North Sea showing that the smoothed well log data fit the telegraph model, which serves to describe the stochastic behavior derived from multiple events. Given its success, we examined its applicability to the earthquake situation albeit at longer wavelengths.

[23] In the coda Q case we are comparing packets of multiples at different lag times over 1-s windows. Thus our method of analysis does not pertain to the low-frequency part of the model because by sampling a 1-s window of coda at twice the lapse times, it does not include the

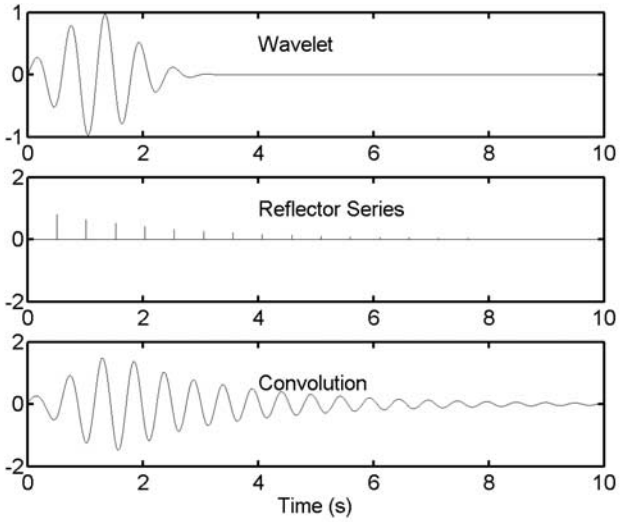

Figure 9b. Synthetic from a lower-frequency wavelet incident on the same reflector series has an order of magnitude lower Q. In each case, intrinsic Q was taken as infinity. Thus the observed apparent Q are due to scattering (trapping) which is much more effective for the high-frequency case.

low frequencies of the initial pulse. Therefore we assume that the high-frequency part of the telegraph model (equation (12)) applies to coda data, which becomes simply

$$Q(\omega) = a_1\omega = \frac{Q_{\min}}{2\omega_c}\omega, \tag{15}$$

where a_1 is a constant to be determined. The final analysis assumed that Q_I is frequency-independent, whereas for Q_S in equation (1) we apply the telegraph model equation (15). Combining equations (1) and (15),

$$\frac{1}{Q_C(\omega)} = \frac{1}{Q_I} + \frac{1}{a_1\omega}. \tag{16}$$

The combined equations (2) and (16) were fit to the $1/Q_C$ (ω) data for each station by varying a_1 in each case and Q_I globally. The Q_I term in equation (16) gives rise to the positive curvature in Figures 5 and 7. A best fit for a global $Q_I \geq 3000$ was higher than expected for previous Q studies [e.g., *Sarker and Abers*, 1998; *Schlotterbeck and Abers*, 2001; *Husker et al.*, 2006; *Hauksson and Shearer*, 2006] which obtain values of about 1000, but those studies do not separate scattering and intrinsic Q. Our total Q range from 100 to 1500, which is similar to those studies. As a check on the high value of intrinsic Q, we took spectral ratios of coda to S waves (Figure 3), which, although scattered, were in general flat enough to be consistent with such large values of intrinsic Q.

[24] The frequency of peak absorption could not be determined from these data, but taking into account the results of *Padhy* [2005], we expect that a value of 0.5 Hz ($\omega_c = 2\pi\, f_c = 2\pi$ 0.5 Hz) is likely to be common across all stations.

[25] A fit of equation (4) to the data revealed, as is well known, that because of covariance it is not possible to separate intrinsic from scattering Q. Letting both vary with frequency gives similar statistics to equation (16). Our justification of equation (16) is that (1) most materials show frequency-independent intrinsic Q and (2) the a priori assumption (based on borehole data) that largest frequency-dependent effects occur in the uppermost crust and the telegraph model is likely to explain the scattering on the basis of its success in exploration geophysics.

[26] Our model implies that the coda are composed of scattered S waves that reverberate in the upper crust and that because scattering is anisotropic and concentrated toward the surface, energy leaks into the lower crust and mantle from where it is lost. A similar model was suggested by *Langston* [1989]. We adopted the telegraph model because of its effectiveness in the reflection seismology industry, but the earthquake problem is at a larger scale than this analog. If we were to consider the full seismogram, including the initial pulse, rather than the 1-s windows of coda, the transfer function between an incident pulse from below the upper crust to that at the surface, including its coda, would then follow the telegraph model in its entirety (equations (2), (12), (13), and (14)). Then the spectrum would include all the low frequencies of the pulse, including DC, which are immune from scattering until wavelengths become comparable to the characteristic wavelengths of the near-surface stack of scattering layers where peak absorption occurs. Smaller wavelengths become trapped, with energy decaying as it leaks downward. If absorption continued to increase at lower frequencies (e.g., equation (16)), microseisms or teleseisms would show much greater decay than is observed.

[27] A simple analogue that illustrates the effect of stratigraphic filtering by the telegraph model is multiple scattering within a layer over a half-space. Consider a high-frequency wavelet (Figure 9a) that reverberates in the layer and sheds energy into the half-space below. The seismogram, calculated as a convolution of the wavelet and reflector series, has a high Q as judged by the number of cycles in exponential folding time (Figure 9a). In this high-frequency case the Q is determined by the number of cycles that fit within the decay time of the reflector series. For a lower-frequency wavelet (Figure 9b), trapping is ineffective, the decay occurs over much fewer cycles, and a much lower Q is inferred. This simple example gives rise to Q increasing with frequency due to scattering. At long wavelengths the layer is virtually invisible, and Q rises again. All frequencies in the coda experience the same attenuation factor, which converted to Q gives the apparent increase of Q with frequency.

[28] Other tests were applied to the magnitude-determined coda data. We searched for a dependence of Q on either azimuth or depth of earthquakes and were unable to resolve any statistically significant variation. In addition, we searched for an annual term using $1/Q(t) = 1/Q_0 + A\cos\omega_y t + B\sin\omega_y t$, where ω_y is the angular frequency corresponding to a calendar year. Of the 232 stations examined, only about six yielded A and B values that are statistically significant at the 95% level. These stations are widely scattered, and such a small number might be expected just because of chance.

7. Conclusions

[29] Deep borehole results on Q suggest that the high-frequency dependence of coda Q is due to scattering multiples in the upper 3 km and the decay is caused by progressive leakage of energy into the transparent lower crust and mantle. We analyzed coda Q envelopes using both magnitude-derived values and waveforms from stations of the Southern California Seismic Network between 2 and 19 Hz. Combined with estimates from earlier studies, we conclude that the upper crust has a transfer function determined by a combination of intrinsic attenuation and scattering described by the telegraph model. The frequency dependence of Q is given by

$$\frac{1}{Q_C(\omega)} = \frac{1}{Q_I} + \frac{2}{Q_{\min}}\frac{\omega/\omega_c}{1+(\omega/\omega_c)^2}. \tag{17}$$

The telegraph model describes an absorption band that has a power law decay (1ω) at high frequencies and a peak absorption $\omega = \omega_c = 2\pi$ (0.5 Hz) related to the average size of scattering layers in the upper crust.

[30] Coda envelopes contain high-frequency multiples which were fit by a high-frequency version of equation (17):

$$\frac{1}{Q_C(\omega)} = \frac{1}{Q_I} + \frac{2}{Q_{\min}}\frac{1}{(\omega/\omega_c)}, \tag{18}$$

which gave Q_C(10 Hz) values between 100 and 1200, similar to previous studies, but suggests $Q_I \geq 3000$.

[31] The Q values at a given site do not exhibit seasonal variation. Also, they do not show significant azimuthal variation, suggesting that coda Q is a good measure of site effects but local multiples must be taken into account, nor do Q values show depth variation. At low frequencies (1–10 Hz), according to this model, the coda Q is dominated by scattering effects and is largely independent of intrinsic Q. The highly heterogeneous spatial variability of coda Q at different stations suggests that the scattering is a local effect in the uppermost crust below the station. If so, it should be repeatable for events arriving along similar paths, which may explain the effectiveness of double differencing that relies on correlations of long wave trains of coda from nearby events. In the vicinity of a station the incident paths tend to coincide and so to sample the same scattering series.

[32] **Acknowledgments.** This work was supported by grants from the UCLA NSF Science and Technology Center for Embedded Networked Sensing (CENS; NSF STC award CCR-0120778) and by the Southern California Earthquake Center (SCEC). SCEC is funded by NSF Cooperative Agreement EAR-0106924 and USGS Cooperative Agreement 02HQAG0008. We thank the Southern California Earthquake Data Center (SCEDC) for supplying the coda and waveform data used in this study. This is SCEC contribution 1078. The reviewers and Associate Editor are thanked for their constructive comments. Ben Wu is thanked for help in the early part of the analysis.

References

Abercrombie, R. E. (1995), Earthquake source scaling relationships from −1 to 5 M_L using seismograms recorded at 2.5 km depth, *J. Geophys. Res.*, *100*, 24,015–24,036.

Abercrombie, R. E. (1997), Near-surface attenuation and site effects from comparison of surface and deep borehole recordings, *Bull. Seismol. Soc. Am.*, *87*(3), 731–744.

Abercrombie, R. E. (1998), A summary of attenuation measurements from borehole recordings of earthquakes: The 10 Hz transition problem, *Pure Appl. Geophys.*, *153*, 475–487.

Abercrombie, R. E. (2000), Crustal attenuation and site effects at Parkfield, California, *J. Geophys. Res.*, *105*, 6277–6286.

Adams, D. A., and R. E. Abercrombie (1998), Seismic attenuation above 10 Hz in southern California from coda waves recorded in the Cajon Pass borehole, *J. Geophys. Res.*, *103*, 24,257–24,270.

Aki, K. (1980), Scattering and attenuation of shear waves in the lithosphere, *J. Geophys. Res.*, *85*, 6496–6504.

Aki, K., and B. Chouet (1975), Origin of coda waves: Source, attenuation, and scattering effects, *J. Geophys. Res.*, *80*, 3322–3342.

Assimaki, D., J. Steidl, and P. C. Liu (2006), Attenuation and velocity structure for site response analysis via downhole seismogram inversion, *Pure Appl. Geophys.*, *163*, 81–118.

Banik, N. C., I. Lerche, and R. T. Shuey (1985a), Stratigraphic filtering, part I: Derivation of the O'Doherty-Anstey formula, *Geophysics*, *50*(12), 2768–2774.

Banik, N. C., I. Lerche, J. R. Resnick, and R. T. Shuey (1985b), Stratigraphic filtering, part II: Model spectra, *Geophysics*, *50*(12), 2775–2783.

Brune, J. N. (1970), Tectonic stress and the spectra of seismic shear waves from earthquakes, *J. Geophys. Res.*, *75*, 4997–5009.

Chernov, L. A. (1960), *Wave Propagation in a Random Medium*, McGraw-Hill, New York.

Dainty, A. M. (1981), A scattering model to explain seismic Q observations in the lithosphere between 1 and 30 Hz, *Geophys. Res. Lett.*, *8*, 1126–1128.

Frankel, A., and R. W. Clayton (1986), Finite difference simulations of seismic scattering: Implications for the propagation of short period seismic waves in the crust and models of crustal heterogeneity, *J. Geophys. Res.*, *91*, 6465–6489.

Frankel, A., and L. Wennerberg (1987), Energy flux model of seismic coda: Separation of scattering and intrinsic attenuation, *Bull. Seismol. Soc. Am.*, *77*(4), 1223–1251.

Hauksson, E., and P. M. Shearer (2006), Attenuation models (Q_p and Q_s) in three dimensions of the southern California crust: Inferred fluid saturation at seismogenic depths, *J. Geophys. Res.*, *111*, B05302, doi:10.1029/2005JB003947.

Hoshiba, M. (1991), Separation of scattering attenuation and intrinsic absorption in Japan with multiple lapse time window analysis from full seismogram envelope, *J. Geophys. Res.*, *98*, 15,809–15,824.

Husker, A. L., M. D. Kohler, and P. M. Davis (2006), Anomalous seismic amplitudes measured in the Los Angeles Basin interpreted as a basin-edge diffraction catastrophe, *Bull. Seismol. Soc. Am.*, *96*(1), 147–164.

Jin, A., K. Mayeda, D. Adama, and K. Aki (1994), Separation of intrinsic and scattering attenuation in southern California using TERRAscope data, *J. Geophys. Res.*, *99*, 17,835–17,848.

Johnson, C. (1979), CEDAR: An approach to the computer automation of short-period local seismic networks, 1. Seismotectonics of the Imperial Valley of southern California, Ph.D. thesis, Calif. Inst. of Technol., Pasadena.

Knopoff, L. (1964), *Q, Rev. Geophys.*, *2*(4), 625–660.

Koyanagi, S., K. Mayeda, and K. Aki (1992), Frequency-dependent site amplification factors using the S-wave coda for the island of Hawaii, *Bull. Seismol. Soc. Am.*, *82*(3), 1151–1185.

Langston, C. A. (1989), Scattering of teleseismic body waves under Pasadena, California, *J. Geophys. Res.*, *94*, 1935–1952.

Magistrale, H., S. Day, R. W. Clayton, and R. Graves (2000), The SCEC southern California reference three-dimensional seismic velocity model version 2, *Bull. Seismol. Soc. Am.*, *90*(6B), S65–S76.

Mayeda, K., S. Koyanagi, M. Hoshiba, K. Aki, and Y. Zeng (1992), A comparative study of scattering, intrinsic, and coda Q^{-1} for Hawaii, Long Valley, and central California between 1.5 and 15.0 Hz, *J. Geophys. Res.*, *97*, 6643–6659.

O'Doherty, R. F., and N. A. Anstey (1971), Reflections on amplitudes, *Geophys. Prospect.*, *19*, 430–458.

Padhy, S. (2005), A scattering model for seismic attenuation and its global applications, *Phys. Earth Planet. Inter.*, *148*(1), 1–12.

Papoulis, A. (1965), *Probability, Random Variables, and Stochastic Processes*, McGraw-Hill, New York.

Pekeris, C. L. (1947), Note on the scattering in an inhomogeneous medium, *Phys. Rev.*, *71*(4), 268–269.

Sarker, G., and G. A. Abers (1998), Comparison of seismic body wave and coda wave measures of Q, *Pure Appl. Geophys.*, *153*, 665–683.

Schlotterbeck, B. A., and G. A. Abers (2001), Three-dimensional attenuation variations in southern California, *J. Geophys. Res.*, *106*, 30,719–30,736.

Wennerberg, L., and A. Frankel (1989), On the similarity of theories of anelastic and scattering attenuation, *Bull. Seismol. Soc. Am.*, *79*(4), 1287–1293.

Wu, R. S., and K. Aki (1988), Multiple scattering and energy transfer of seismic waves: Separation of scattering effect from the intrinsic attenuation, part II: Application of the theory to Hindu Kush region, *Pure Appl. Geophys.*, *128*, 49–80.

Zeng, Y., F. Su, and K. Aki (1991), Scattering wave energy propagation in a medium with randomly distributed isotropic scatterers: 1. Theory, *J. Geophys. Res.*, *96*, 607–619.

R. W. Clayton, Seismological Laboratory, California Institute of Technology, 1200 California Blvd. 252-21, Pasadena, CA 91125, USA. (clay@gps.caltech.edu)

P. M. Davis, Department of Earth and Space Sciences, UCLA, 595 Circle Drive East, Los Angeles, CA 90095, USA. (pdavis@ess.ucla.edu)